RSC Advances

PAPER

Cite this: *RSC Adv.*, 2021, **11**, 4555

Design, synthesis and biological evaluation of 2-quinolyl-1,3-tropolone derivatives as new anti-cancer agents†

Evgeniy A. Gusakov,‡[a] Iuliia A. Topchu,‡[bc] Aleksandra M. Mazitova,‡[bd] Igor V. Dorogan,[a] Emil R. Bulatov,[b] Ilya G. Serebriiskii,[be] Zinaida I. Abramova,[b] Inna O. Tupaeva,[a] Oleg P. Demidov,[f] Duong Ngoc Toan,[g] Tran Dai Lam,[h] Duong Nghia Bang,[i] Yanis A. Boumber,*[bc] Yurii A. Sayapin*[j] and Vladimir I. Minkin[a]

Received 17th December 2020
Accepted 12th January 2021

DOI: 10.1039/d0ra10610k

rsc.li/rsc-advances

Tropolones are promising organic compounds that can have important biologic effects. We developed a series of new 2-quinolyl-1,3-tropolones derivatives that were prepared by the acid-catalyzed reaction of 4,7-dichloro-2-methylquinolines with 1,2-benzoquinones. 2-Quinolyl-1,3-tropolones have been synthesized and tested for their anti-proliferative activity against several human cancer cell lines. Two compounds (**3d** and mixture B of **3i–k**) showed excellent activity against six cancer cell lines of different tissue of origin. The promising compounds **3d** and mixture B of **3i–k** also demonstrated induction of apoptotic cell death of ovarian cancer (OVCAR-3, OVCAR-8) and colon cancer (HCT 116) cell lines and affected ERK signaling. In summary, 2-quinolyl-1,3-tropolones are promising compounds for development of effective anticancer agents.

1. Introduction

Today, cancer remains one of the leading causes of death in most parts of the world and is a serious obstacle to increasing life expectancy in most countries.[1] Ovarian cancer is the seventh most common type of cancer in women worldwide[2] and one of the most common type so gynecological malignant tumors.[3] Colon cancer is both the third most common cancer and the third most common cause of death among cancer patients.[1] The standard systemic therapy for ovarian cancer is platinum chemotherapy doublet (cisplatin and carboplatin)[4] in combination with taxanes (paclitaxel or docetaxel) and sometime doxorubicin,[5] while for colon cancer, the most effective chemotherapy strategy is chemotherapy doublet with oxaliplatin, combined with either 5-fluorouracil or irinotecan.[6]

However, platinum compounds have serious side effects such as nausea and vomiting, nephrotoxicity, ototoxicity, neurotoxicity, cytopenia and muscle wasting.[7] In addition, in metastatic settings, very often, recurrent ovarian or colon cancers commonly acquire resistance to platinum drugs.[8,9] All these factors negatively affect both the quality of life of cancer patients and their survival rate. Therefore, the search and development of new medicinal compounds with antitumor activity remains an urgent task.

Derivatives of tropolones are a class of promising organic compounds that can act as new pharmaceutical anti-inflammatory and antitumor agents. Currently, there is an increased interest in tropolone alkaloids, since many of them have a wide range of pharmacological activity. For example, some of the best-known representatives are colchicine, colchamine and β-thujaplicin (hinokitiol), which have antitumor, antibacterial, antiviral, antifungal, anti-inflammatory and antioxidant properties.[10–12] In particular, high anti-bacterial and anti-inflammatory effects of natural alkaloids cordytropolone and stipitalide against *Propionibacterium acnes* have been

[a]*Institute of Physical and Organic Chemistry, Southern Federal University, Rostov-on-Don, 344090, Russia*
[b]*Kazan Federal University, Kazan, 420008, Russia*
[c]*Robert H Lurie Comprehensive Cancer Center, Division of Hematology/Oncology at the Department of Medicine, Feinberg School of Medicine, Northwestern University, 303 E. Superior Street, Chicago, IL, 60611, USA. E-mail: yanis.boumber@northwestern.edu*
[d]*Cedars-Sinai Medical Center, Department of Medicine, Los Angeles, CA, 90048, USA*
[e]*Fox Chase Cancer Center, Philadelphia, PA, 19111, USA*
[f]*North Caucasus Federal University, Stavropol, 355009, Russia*
[g]*Thai Nguyen University of Education, 20 Luong Ngoc Quyen, Thai Nguyen 24000, Vietnam*
[h]*Institute for Tropical Technology, Vietnam Academy of Science and Technology, Hanoi, 10000, Vietnam*
[i]*Thai Nguyen University of Sciences, Tan Thinh Ward, Thai Nguyen 24000, Vietnam*
[j]*Federal Research Centre the Southern Scientific Centre of the Russian Academy of Sciences, Chekhov Ave., 41, Rostov-on-Don, 344006, Russia. E-mail: sayapin@ipoc.sfedu.ru*

† Electronic supplementary information (ESI) available: Detailed experimental data (Fig. S1–S20 and Tables S1–S24). CCDC 2040512. For ESI and crystallographic data in CIF or other electronic format see DOI: 10.1039/d0ra10610k

‡ These authors contributed equally.

recently shown.[13] 3-Isopropenyl-tropolone has high activity against antibiotic-resistant bacteria *Staphylococcus aureus*,[14] while hinokitiol was effective against MRSA, *Aggregatibacter actinomycetemcomitans*, *Streptococcus mutans*, and *Candida albicans*.[15] The antiviral properties of natural hydroxylated tropolones (β-thujaplicinol, manicol) against HIV-1.16 have also been established.[16]

There are a number of studies demonstrating in more detail the antitumor activity of hinokitiol. Hinokitiol blocks DNA homology recombination and repair process in breast cancer and osteosarcoma cells and is able to radiosensitize these cells and increase apoptosis in combination with PARP inhibitor.[17] Hinokitiol also exhibits antitumor effect in malignant lymphoma and myeloma cells by inducing caspase-dependent apoptosis.[18,19] Moreover, it can inhibit migration of melanoma cells.[20] An equally interesting fact exists about the relationship between hinokitiol and DNA methylation in colon cancer cells. Hinokitiol can block DNA methylation *via* DNMT1 inhibition that may open up the prospects for its use as a new DNMT1 inhibitor.[21]

Thus, tropolone derivatives have multi-target biologic and anti-tumor activity in various types of cancer cells and are therefore of interest for further studies.

Synthetic methods for the preparation of analogs of natural tropoids with high biological activity have been described in detail earlier.[22] However, related 1,3-tropolone systems with heterocyclic fragments have hardly been studied.

We have previously reported on the cytotoxic activity of halogenated derivatives of [benzo[*b*][1,4]oxazepino[7,6,5-de] quinolyl]-1,3-tropolones. The most significant result in the investigated series was shown by 2-[7-acetyl-9,11-di(*tert*-butyl)-4-methyl-5-chlorobenzo[*b*][1,4]oxazepino[7,6,5-de]-quinolyl]-5,6,7-trichloro-1,3-tropolone, inhibited the growth of breast cancer cells MCF-7 at IC_{50} concentration of 12.96 μg ml^{-1}, as well as of epidermoid cells KB, lung cancer cells Lu and liver cancer cells Hep-G2 at IC_{50} concentrations >128 μg ml^{-1}.[23] In the present work, we report on the synthesis, molecular structure and cytotoxic properties of the novel 2-quinolin-2-yl-1,3-tropolones.

2. Results and discussion

2.1 Chemistry

Previously, it was established that acid-catalyzed reactions methylene-active heterocycles (substituted benzazoles or 3,3-dimethylindolines,[24] quinolines,[25] quinoxalines,[26] benzoxazinones,[27] quinazolinone[28]) with 1,2-benzoquinone derivatives proceed with the expansion of the *o*-quinone ring and can lead to the formation of 2-hetaryl-1,3-tropolones. The yields of the final 2-hetaryl-1,3-tropolones can vary in the particular series of methylene active heterocyclic compound or 1,2-benzoquinone depending on the substituents. The most optimal condition for the synthesis of 2-hetaryl-substituted 1,3-tropolones is to carry out the reaction at moderate temperatures (60–80 °C) in acetic acid solution.

In this work, we used 2,8-dimethyl-4,7-dichloroquinoline (**1a**) and its 5-nitro derivative (**1b**) as the methylene-active heterocycle, and 3,5-di(*tert*-butyl)-1,2-benzoquinone (**2a**), 4,6-di(*tert*-butyl)-3-nitro-1,2-benzoquinone (**2b**), 4,6-diisopropyl-3-nitro-1,2-benzoquinone (**2c**),[29] 3,4,5,6-tetrachloro-1,2-benzoquinone (**2d**) as the initial 1,2-benzoquinones. The preparation of 2-quinolyl-1,3-tropolone derivatives **3** is presented in Scheme 1.

It has been established that the interaction of quinolines **1a**, **b** with a twofold excess of quinones **2a–c** leads to the formation of the corresponding 2-quinolyl-1,3-tropolones **3a–f** (method A). However, in the reaction of **1a** with quinone **2c**, tropolone **3g** is formed along with tropolone **3f** in small amounts (10%). Reaction products **3f** and **3g** were isolated from the reaction mixture by column chromatography. On the other hand, reaction **1b** with quinone **2c** (method A) proceeded with the formation of only tropolone **3e**.

Refluxing **1a** with an equivalent amount of **2d** in dioxane (method B) leads to the formation of 2-quinolyl-5,6,7-trichloro-1,3-tropolone **3h**. However, the reaction of 5-nitro derivative **1b** with **2d** gives rise the mixture of three polychloro-substituted tropolones: 5,6,7-trichloro-1,3-tropolone **3i**, 4,5,6,7-tetrachloro-1,3-tropolone **3j** and 4,5,6-trichloro-1,3-tropolone **3k** (Scheme 2) in a ratio of 55, 30, and 15%, respectively (mixture B of **3i–k**). Since it was impossible to separate a mixture of tropolones **3i–k** by thin layer or column chromatography, the ratio of the mixture has been determined from the integrated signal intensity of OH-group protons.

Carrying out the reaction **1b** (1 eq.) with **2d** (2 eq.) under milder conditions in acetic acid (method A) leads to a change in the ratio of the mixture of polychlorotropolones (35% (**3i**), 55% (**3j**) 10% (**3k**)). Since the mixture B of tropolones **3i–k** can easily be obtained synthetically, mixture of B was investigated further for the anticancer activity.

The mechanism of formation of the tropolone system **3** was studied earlier by theoretical methods. The multistep reaction includes aldol condensation with the formation of intermediate **A**, cyclization of **A** into the norcaradiene derivative **B**, and rearrangement of **B** into the dihydrotropolone **C**. Oxidation of the latter with an excess of the initial 1.2-benzoquinone **2** leads to 1,3-tropolones **3a–f** (method A).

Interaction of 4,7-dichloro-2-methylquinolines **1a** with 4,6-diisopropyl-3-nitro-1,2-benzoquinone **2c** gives rise two competing processes: the formation of tropolone **3f** and the reaction of nitrous acid elimination in **C**, accompanied by 1,3-sigmatropic shift of the hydrogen atom, which ultimately leads to the formation of 1,3-tropolone **3g**.

o-Quinone ring expansion upon refluxing **1a**,**b** with 3,4,5,6-tetrachloro-1,2-benzoquinone **2d** (method B) proceeds according to a similar mechanism, but in this case intermediate **C** under goes dehydrochlorination, and as a result tropolones **3h** and the mixture of tropolones **3i**, **k** were obtained. The formation of the isomeric 4,5,6-trichloro-1,3-tropolone **3k** was observed only in the case of the reaction of **2d** with **1b**. Tropolone **3j** is formed by both method **A** and method **B** due to the competing oxidation reaction of intermediate **C** with 1,2-benzoquinone **2d**.

The structure of the compounds **3a–k** that we obtained was confirmed by ^{1}H NMR and IR spectroscopy and mass

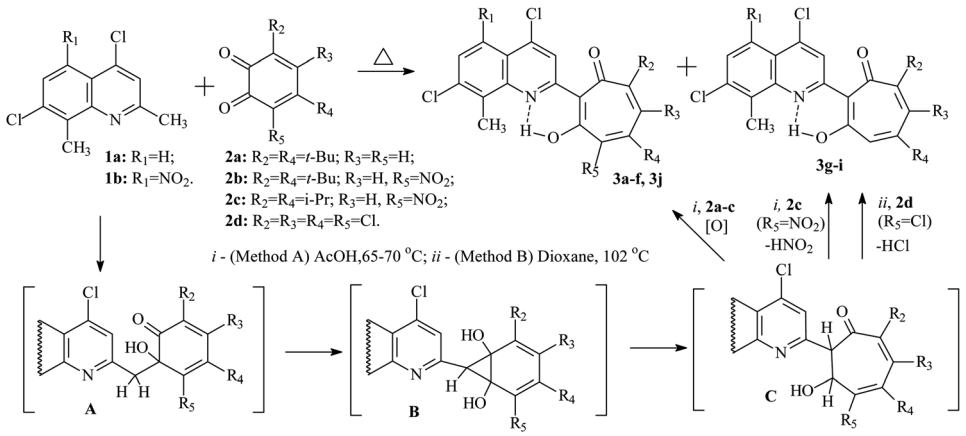

Scheme 1 Synthesis of 2-quinolyl-1,3-tropolone derivatives **3** by an alternative pathway of the reaction.

spectrometry data. In the ^{1}H NMR spectra of compounds **3a–j**, the signal of the proton of the hydroxyl group, which forms a strong hydrogen bond with the quinoline nitrogen atom in the first position, closing the six-membered chelate ring, is observed in the downfield region δ_H 17–19 ppm in the form of a narrow singlet peak. ^{1}H NMR spectrum of polychlorinated tropolones **3i–k** showed in a weak field the presence of three signals of OH protons – groups 18.61 ppm (**3i**), 17.92 ppm (**3j**), 17.22 ppm (**3k**). Signals of protons of the tropolone cycle appear at 7.19 ppm (**3i**) and 7.33 ppm (**3k**). The HRMS (ESI) (*m*/*z* [M–H]) mass spectrum of tropolones **3i–k** confirms the presence of compounds with molecular weights of 476.8777, which corresponds to **3i**,**k** and 510.8380, which corresponds to **3j**. The synthesis conditions and some physicochemical data of the obtained compounds **3a–j** are shown in Table 1.

The structure of **3c** was established by X-ray diffraction analysis and is shown in Fig. 1. As a result of the prototropic rearrangement, the hydrogen atom is confidently localized at the nitrogen atom N(1) at a distance of 0.98(2) Å and participates in the formation of intramolecular hydrogen bond with the oxygen atom of the carbonyl group of tropolone with the following parameters: O(2)–C(3) = 1.2785 (15) Å, H(1)···O(2) −1.567 Å, the angle N(1)–H(1)–O(2) in the cycle formed by the intramolecular hydrogen bond is 149.78. The bond lengths of the aminoenone system N(1)–C(8) = 1.3464(16) Å and C(8)–C(2) = 1.4454(16) Å are close in their absolute values to those for the fixed diketone form in 2-substituted *N*-methylquinoline[30] (1.353 Å and 1.443 Å, respectively. Deposition number 1864613). This indicates the realization in the crystalline phase the aminoenone form (NH) of tropolone **3c** (Fig. 1a). It should be noted that the tropolone cycle in the crystal takes on the "bath" conformation (Fig. 1b).

Compounds **3** can exist in solution in two tautomeric (OH) and (NH) forms (Scheme 3). The thermodynamic equilibrium between them in the gas phase and polar solvent (DMSO) has been studied by theoretical methods (DFT) (Table 2) (Fig. S1–S3, Tables S1–S22, ESI†).

According to theoretical estimates, the main influence on the equilibrium of (NH) and (OH) tautomeric forms of tropolone derivatives is exerted, on the one hand, by the donor–acceptor properties of the quinoline and tropolone fragments, and on the other, by the polarity of the environment. Variations of these factors make it possible to change the equilibrium of these isomers over a wide range (Table 2).

An acceptor substituent (nitro group) in the quinoline moiety of **3** stabilizes the (OH) isomer. On the contrary, increase of the medium polarity stabilizes the (NH) form to a greater extent. Replacement of *tert*-butyl substituents in the tropolone fragment with isopropyl substituents does not significantly affect the results.

The introduction of the nitro group into the tropolone fragment stabilizes (NH) isomer. In the polar solvent (DMSO), this effect is further enhanced. The introduction of the nitro group into both tropolone and quinoline fragments of molecules (compounds **3d** and **3e**) also stabilizes the (NH) isomer, but to a lesser extent than one nitro group in the tropolone part of the molecule. This indicates that acceptor substituents in the quinoline and tropolone fragments partially compensate for

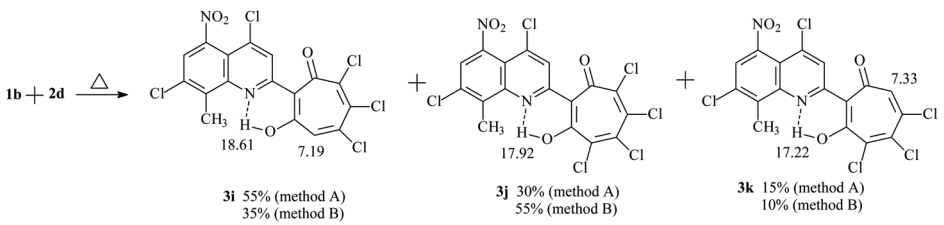

Scheme 2 Formation of the mixture of three polychloro-substituted 1,3-tropolones **3i–k**.

Table 1 Novel derivatives of 2-(7-chloro-2-quinolyl)-1,3-tropolones **3**

Compd	Structure	Reaction conditions	Yield (%)	Melting point (°C)	^{1}H $\delta_{OH(NH)}$ (ppm)
3a	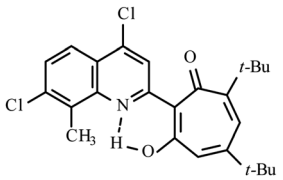	Method A: AcOH, 65–70 °C, **1a** (1 eq.)/**2a** (2 eq.)	63	189–190	18.77
3b	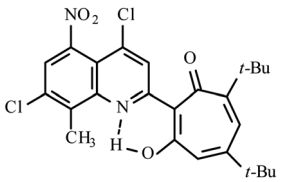	Method A: AcOH, 65–70 °C, **1b** (1 eq.)/**2a** (2 eq.)	47	264–265	17.57
3c	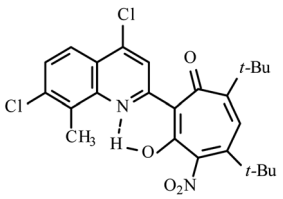	Method A: AcOH, 65–70 °C, **1a** (1 eq.)/**2b** (2 eq.)	30	236–237	18.17
3d	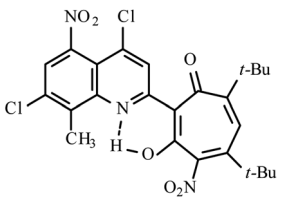	Method A: AcOH, 65–70 °C, **1b** (1 eq.)/**2b** (2 eq.)	77	254–255	18.35
3e	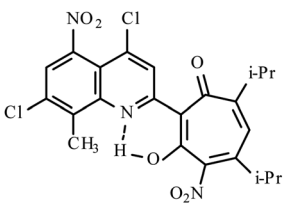	Method A: AcOH, 65–70 °C, **1b** (1 eq.)/**2c** (2 eq)	28	255–256	19.19
3f	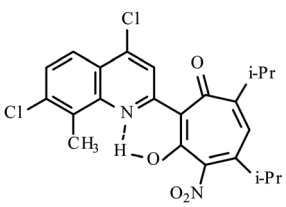	Method A: AcOH, 65–70 °C, **1a** (1 eq.)/**2c** (2 eq.)	51	189–190	19.18
3g	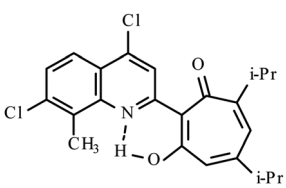		10	147–148	19.01
3h	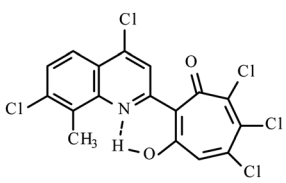	Method B: dioxane, 102 °C, **1a** (1 eq.)/**2d** (1.1 eq.)	72	275–276	19.02

Table 1 (*Contd.*)

Compd	Structure	Reaction conditions	Yield (%)	Melting point (°C)	^{1}H $\delta_{OH(NH)}$ (ppm)
***Mixture* 3i, 3j, 3k**	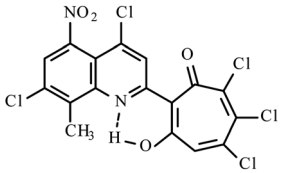	Method A: AcOH, 65–70 °C, **1b** (1 eq.)/**2d** (2 eq.)	55(A)[a]	197–200[A]	18.61[3i]
	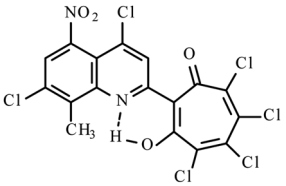	Method B: dioxane, 102 °C, **1b** (1 eq.)/**2d** (1.1 eq.)	46(B)[b]	192–193[B]	17.92[3j]
	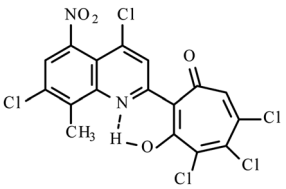				17.22[3k]

[a] Method A (mixture in a ratio of **3i** (35%), **3j** (55%), **3k** (10%)). [b] Method B(mixture in a ratio of **3i** (55%), **3j** (30%), **3k** (15%)).

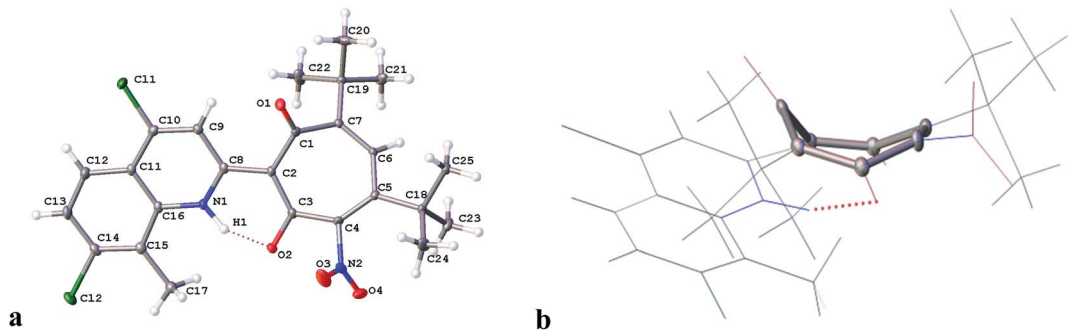

Fig. 1 Molecular structure of 5,7-di(*tert*-butyl)-2-(4,7-dichloro-8-methyl-2-quinolyl)-4-nitro-1,3-tropolone **3c** with representation of the atoms by thermal vibration ellipsoids of 50% probability (a); a tropolone cycle in a crystal in the "bath" conformation (b).

each other's influence and, on the other hand, demonstrates a higher effectiveness of acceptor substituents in the tropolone moiety. Stabilization of the (NH) isomer is also observed upon replacement of *tert*-butyl substituents in the tropolone fragment with chlorine atoms (compounds **3h**, **3i**), which is consistent with the general properties of the tautomeric equilibrium in these systems mentioned above.

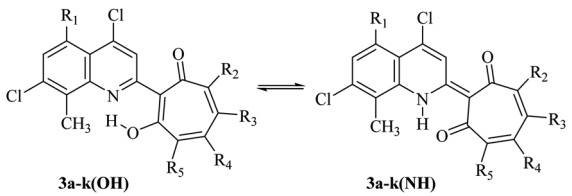

Scheme 3 Intramolecular proton transfer in compounds **3a–k**.

2.2. Biology

2.2.1. *In vitro* anti-proliferative activity of tropolone compounds 3a–h and tropolone mixture B (3i–k). First, the anti-proliferative activity of all novel tropolone compounds **3a–h** and mixture B of **3i–k** was tested out in parallel against six human cancer cell lines (lung cancer: A549 and H441, ovarian cancer: OVCAR-3 and OVCAR-8, colon cancer: HCT 116, and pancreatic cancer: Panc-1) using Alamar Blue Cell Viability Reagent (Invitrogen, UK).

Table 2 Total energies with zero-point energy correction E_{tot} + ZPE (au) and relative energies ΔE (kcal mol^{-1}) of (NH) and (OH) isomers of tropolone derivatives **3a–j** in the gas phase (g) and DMSO solution (s) according to the PBE0/6–311 + G (d, p) calculations

Structure	E_{tot} + ZPE (g)	ΔE (g)	E_{tot} + ZPE (s)	ΔE (s)
3a (NH)	−2092.705668	0.0	−2092.715974	0.0
3a (OH)	−2092.707205	−0.96	−2092.716625	−0.41
3b (NH)	−2297.039006	0.0	−2297.053321	0.0
3b (OH)	−2297.041444	−1.53	−2297.055267	−1.22
3c (NH)	−2297.041242	0.0	−2297.056554	0.0
3c (OH)	−2297.040005	0.78	−2297.053547	1.89
3d (NH)	−2501.373627	0.0	−2501.392772	0.0
3d (OH)	−2501.373616	0.01	−2501.390877	1.19
3e (NH)	−2422.890683	0.0	−2422.909876	0.0
3e (OH)	−2422.890567	0.07	−2422.908419	0.91
3f (NH)	−2218.557968	0.0	−2218.573183	0.0
3f (OH)	−2218.557252	0.45	−2218.57104	1.34
3g (NH)	−2014.218773	0.0	−2014.229307	0.0
3g (OH)	−2014.220275	−0.94	−2014.230029	−0.45
3h (NH)	−3157.133771	0.0	−3157.144041	0.0
3h (OH)	−3157.133633	0.09	−3157.142118	1.21
3i (NH)	−3361.465409	0.0	−3361.479782	0.0
3i (OH)	−3361.466531	−0.70	−3361.479323	0.29
3j (NH)	−3820.926859	0.00	−3820.941783	0.00
3j (OH)	−3820.925688	0.73	−3820.938795	1.87
3k (NH)	−3361.463126	0.00	−3361.478029	0.00
3k (OH)	−3361.462296	0.52	−3361.475645	1.50

This reagent contains non-toxic resazurin-based solution that is blue in color and non-fluorescent, upon entering living cells, resazurin is reduced to resorufin, a compound that is red in color and highly fluorescent. Conversion of resazurin to resorufin is used as a means to measure relative numbers of living cells. The effect of the test compounds was evaluated at concentrations up to 5 μM. This is due to the low solubility of compounds **3a–h** and mixture B of **3i–k** in DMSO, and due to the fact that an increase in DMSO amount can lead to the toxic effect of the solvent on cell lines under study, that can result in distortion of experimental findings. For additional controls, we used well-known analogue compound of the tropolone series, hinokitiol, and a widely used chemotherapy drug cisplatin. The IC_{50} values are summarized in Table 3, with the values shown representing the average of at least three independent experiments. A dash means that the compounds did not show antiproliferative activity in cell lines tested in the concentration range up to 5 μM. Representative IC_{50} curves for **3d** and mixture B (of **3i–k**) the cell lines in three cell lines are shown in Fig. S4 (see ESI†).

The IC_{50} values of compounds **3a**, **3b**, **3e**, **3g**, **3f** did not fall within the concentration range up to 5 μM. In contrast, the compounds **3h** and **3c** showed antiproliferative activity against the OVCAR-8, OVCAR-3 and H441 cell lines, and the IC_{50} values of these compounds were lower than the values for cisplatin and hinokitiol. Compounds **3d** and mixture B of **3i–k** demonstrated broad inhibitory activity against all six cell lines. The IC_{50} values ranged from 0.95 to 3.93 μM and from 0.51 to 1.98 μM for **3d** and mixture B of **3i–k** respectively. In addition, the antiproliferative activities of these compounds against OVCAR-3, OVCAR-8 and HCT 116 were generally better than against other cell lines (Table 3).

Since **3d** and mixture B of **3i–k** compounds showed the broadest range of biologic activity across all 6 cancer cell lines, we next focused our biologic studies on these tropolones. As a proof of concept, we decided to focus on HCT 116 colon and OVCAR-3 and OVCAR-8 ovarian cancer cell lines. Nowadays, the standard first-line therapy for both of these two types of cancer includes platinum-based doublet drug combinations, but the majority of patients ultimately experience resistance to platinum drugs or dose-limiting toxicities. Furthermore, unlike in lung cancer, immunotherapy is generally ineffective for the majority of ovarian and colon cancers, therefore only a few advances occurred in these disease in these disease in the last decades. This latter fact led us to continue looking for ways to improve treatments for these two common, yet difficult to treat types of cancers.

For the next set of biological experiments, we used compounds at IC_{50} and IC_{25} concentration values. The values IC_{50} of **3d** compound for OVCAR-3, OVCAR-8 and HCT 116 were 3.93 μM, 1.33 μM and 2.15 μM, respectively. At the same time, IC_{50} of mixture B **3i–k** compound for these three cell lines were 0.63 μM, 1.98 μM and 1.15 μM, respectively.

Analyzing the structure and biological activity of compounds **3**, we decided that the most active compounds in the series of 2-quinoline-1,3-tropolones against various cancer cell lines (H441, A549, OVCAR-3, OVCAR-8, HCT 116, Panc-1) are

Table 3 IC_{50} values of the designed compounds, including **3d** and mixture B of **3i–k** (μM) in various human cancer cell lines

Cell line	**3a, 3b, 3g, 3f, 3e**	**3h**	**3c**	**3d**	Mixture B of **3i–k**	Cisplatin[e]	Hinokitiol[e]
OVCAR-8[a]	>5	2.62	>5	1.33	1.98	3.75	>5
OVCAR-3[a]	>5	4.73	3.93	3.93	0.63	5.10	>5
H441[b]	>5	1.35	2.62	0.97	0.70	3.74	1.97
A549[b]	—	—	—	4.05	1.61	4.16	>5
HCT 116[c]	—	—	—	2.15	1.15	4.22	>5
Panc-1[d]	—	—	—	0.95	0.51	3.25	>5

[a] Human ovarian cancer. [b] Human lung cancer. [c] Human colon cancer. [d] Human pancreatic cancer. [e] Comparison control drugs were cisplatin and hinokitiol.

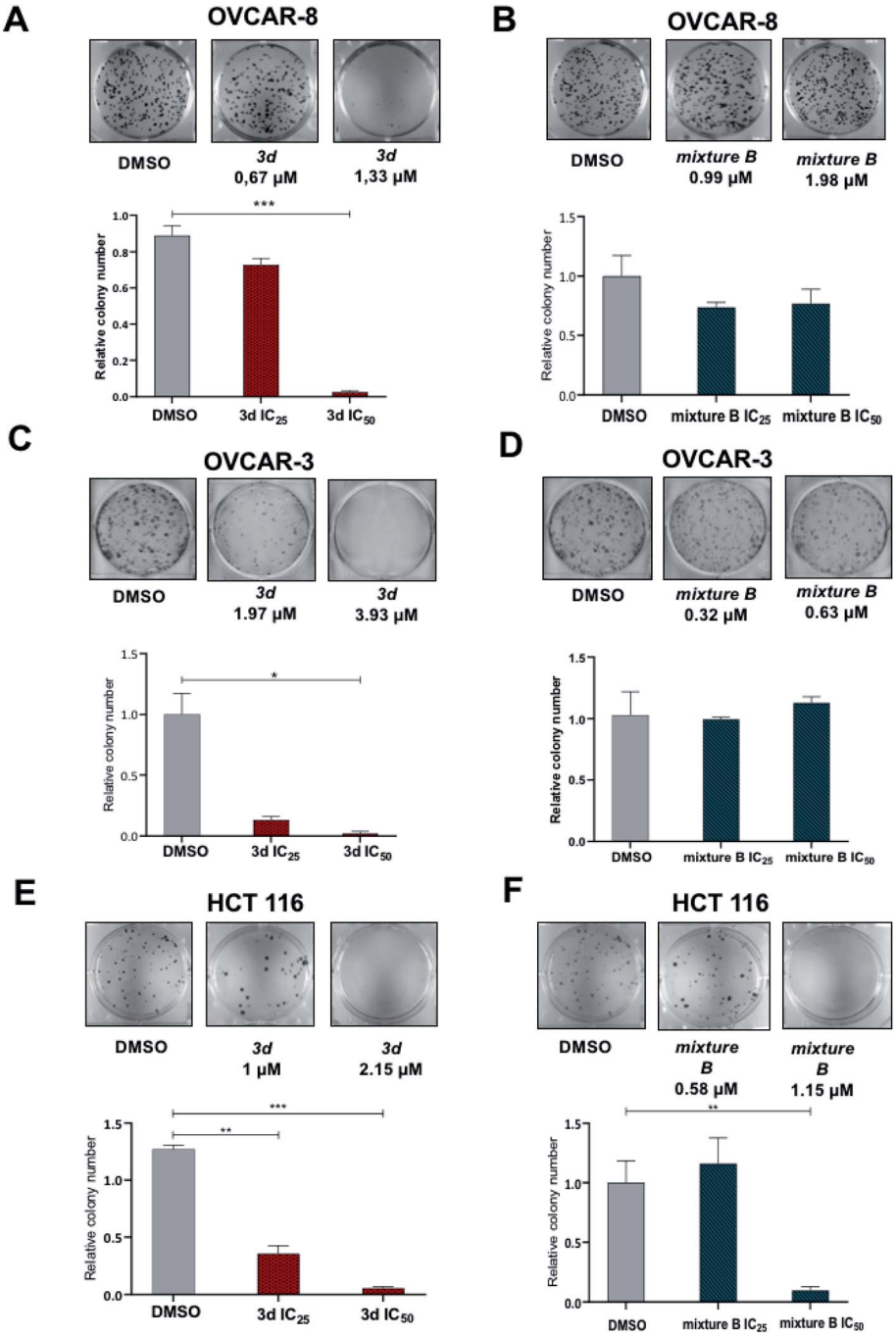

Fig. 2 Effect of **3d** and mixture B of **3i–k** tropolones at IC_{25} and IC_{50} concentrations on colony formation ability of ovarian and colon cancer cells. (A) OVCAR-8 under **3d** treatment for 7 days; (B) OVCAR-8 under mixture B (**3i–k** treatment for 7 days); (C) OVCAR-3 under **3d** treatment for 7 days; (D) OVCAR-3 under mixture B of treatment of **3i–k** for 7 days; (E) HCT 116 under **3d** treatment for 7 days; (F) HCT 116 under mixture B of treatment of **3i–k** for 7 days.

tropolones containing acceptor groups (NO2, Cl) in the periphery of the tropolone ring – 5,7-di(*tert*-butyl)-2-(4,7-dichloro-8-methyl-2-quinolyl)-4-nitro-1,3-tropolone **3c**, 5,7-di(*tert*-butyl)-2-(4,7-dichloro-8-methyl-5-nitro-2-quinolyl)-4-nitro-1,3-tropolone **3d** and polychlorinated derivatives – 2-(4,7-dichloro-8-methyl-2-quinolyl)-5,6,7-thrichloro-1,3-tropolone **3h** and mixture B of **3i–k.** These tropolones, according to quantum chemical calculations, are in the tautomeric aminoenone form **3** (NH). It is likely that the tautomeric **3** (NH)-form is involved in the mechanisms of inhibition of the growth of cancer cells. Despite the fact that compounds **3e,f** (5,7-di-isopropyl) are also in the aminoenone form **3** (NH), like their structural analogs **3c,3d** (5,7-di-(*tert*-butyl)) the IC_{50} values of compounds **3e,f** turned out to be higher than 5 μM. And tropolones **3c**, **3d** with bulkier *tert*-butyl substituents at positions 5 and 7 of the

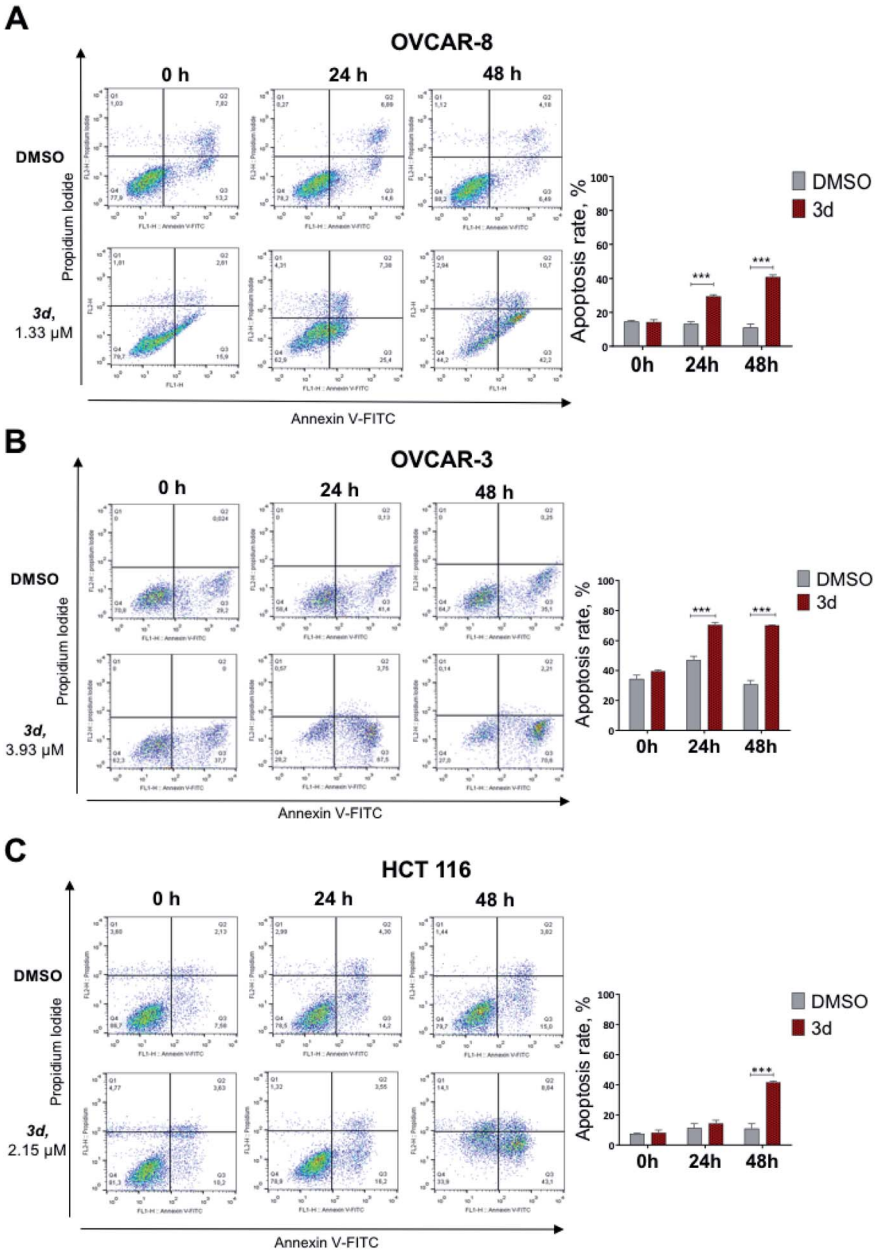

Fig. 3 Effect of **3d** on apoptosis induction in ovarian and colon cancer cell lines. Cells were treated **3d** at indicated concentration, or with DMSO. Flow cytometry results after at 0 h, 24 h, 48 h using Annexin V and propidium iodide are shown for OVCAR-8 (A), OVCAR-3 (B) and HCT 116 (C) cell line.

tropolone ring showed the best results in inhibiting cancer cells in this series of compounds under study.

2.2.2. Tropolone compound 3d and tropolone mixture B (3i–k) inhibit colony formation of human ovarian and colon cancer cells. Since **3d** and mixture B of **3i–k** compounds showed the broadest range of biologic activity across all six cancer cell lines, we next focused our biologic studies on these compounds. We decided to focus on HCT 116 colon and OVCAR-3 and OVCAR-8 ovarian cancer cell lines, for a proof of concept *in vitro* study. Colony formation assay was performed to verify clonogenic ability of cells with the focus on compound **3d** and mixture B of **3i–k** compounds treatment for 7 days. These cancer cell lines were treated with these two compounds at IC_{25} and IC_{50} concentrations. As shown in Fig. 2, treatment of these cells leads to significantly decreased clonogenic capacity in all three cell lines tested with compound **3d** (Fig. 2A, C and E). In contrast, as shown in Fig. 2B, D and F, mixture B of **3i–k** did not significantly inhibit the colony formation ability of ovarian cancer cells as measured by the cytotoxicity test, while the colony formation of HCT 116 colon cancer cells is significant inhibited by mixture B of **3i–k** (Fig. 2F). This indicates that colon cancer cells are more sensitive to mixture B of **3i–k** than ovarian cancer cells.

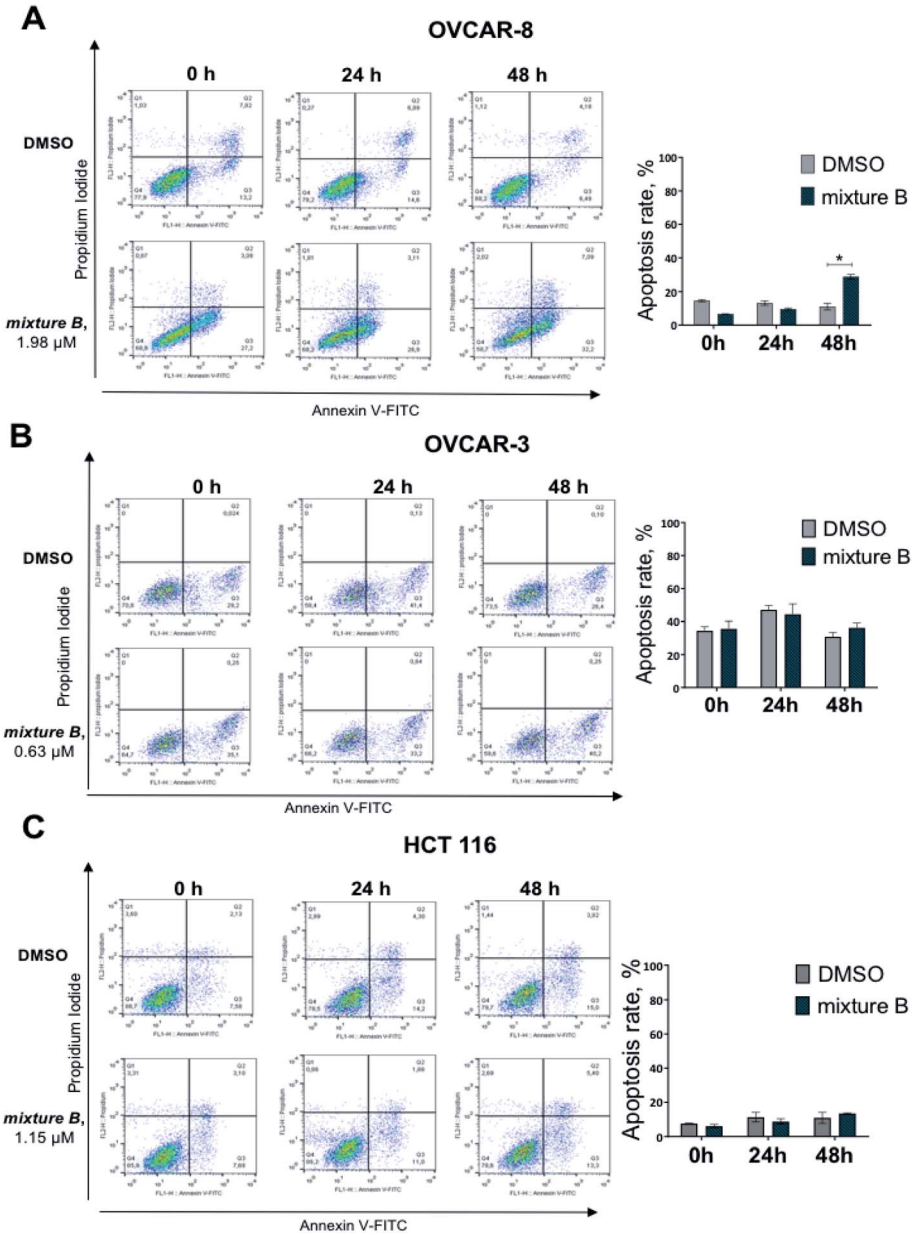

Fig. 4 Effect of mixture B of **3i–k** on apoptosis induction in ovarian and colon cancer cell lines. Flow cytometry results after at 0 h, 24 h, 48 h treatment using Annexin V and propidium iodide are shown for OVCAR-8 (A), OVCAR-3 (B) and HCT 116 (C) cell line.

2.2.3. Compound 3d and tropolone mixture B (3i–k) induce apoptosis in ovarian and colon cancer cell lines. Proliferation and clonogenic effects suggested that these **3d** and mixture B (**3i–k**) compounds could induce apoptosis in cancer cells. To confirm if cancer cells proliferation effects are due to apoptosis type of cell death triggered by **3d** and mixture B (**3i–k**) compounds, we treated ovarian and colon cancer cells by **3d** or mixture B for 24 and 48 h and then stained cells with Annexin V-FITC and propidium iodide (PI) and then analyzed by flow cytometry. DMSO control induced significant apoptosis, especially in OVCAR-8 cell line. However, **3d** compound induced significantly more apoptosis. The percentages of apoptosis in OVCAR-8 cells treated with **3d** were for 24 and 48 hours 26.77 ± 1.8% and 46.2 ± 1.8%, respectively (Fig. 3A). The OVCAR-3 cell line demonstrated a 28.9 ± 2.8% increase (p-value < 0.0001) in the number of apoptotic cells from control by 24 hours under **3d** treatment. As shown in Fig. 3B, this effect also continued at 48 hours compound exposure time point (Fig. 3B). HCT 116 colon cancer cells also show high apoptotic level relative to DMSO at 48 hours exposure at 50.87 ± 9.2% (p-value < 0.0001) (Fig. 3C).

Under the treatment with mixture B (**3i–k**), only OVCAR-8 cells had significantly more (p-value < 0.0001) apoptotic cells relative to DMSO. The total numbers of late (Annexin-V+/PI+) apoptotic cells after the 48 hours treatment increased to 32.2 ± 1.7%. However, in OVCAR-3 and HCT 116 cells, apoptosis was no different and similar to control DMSO treatment (Fig. 4).

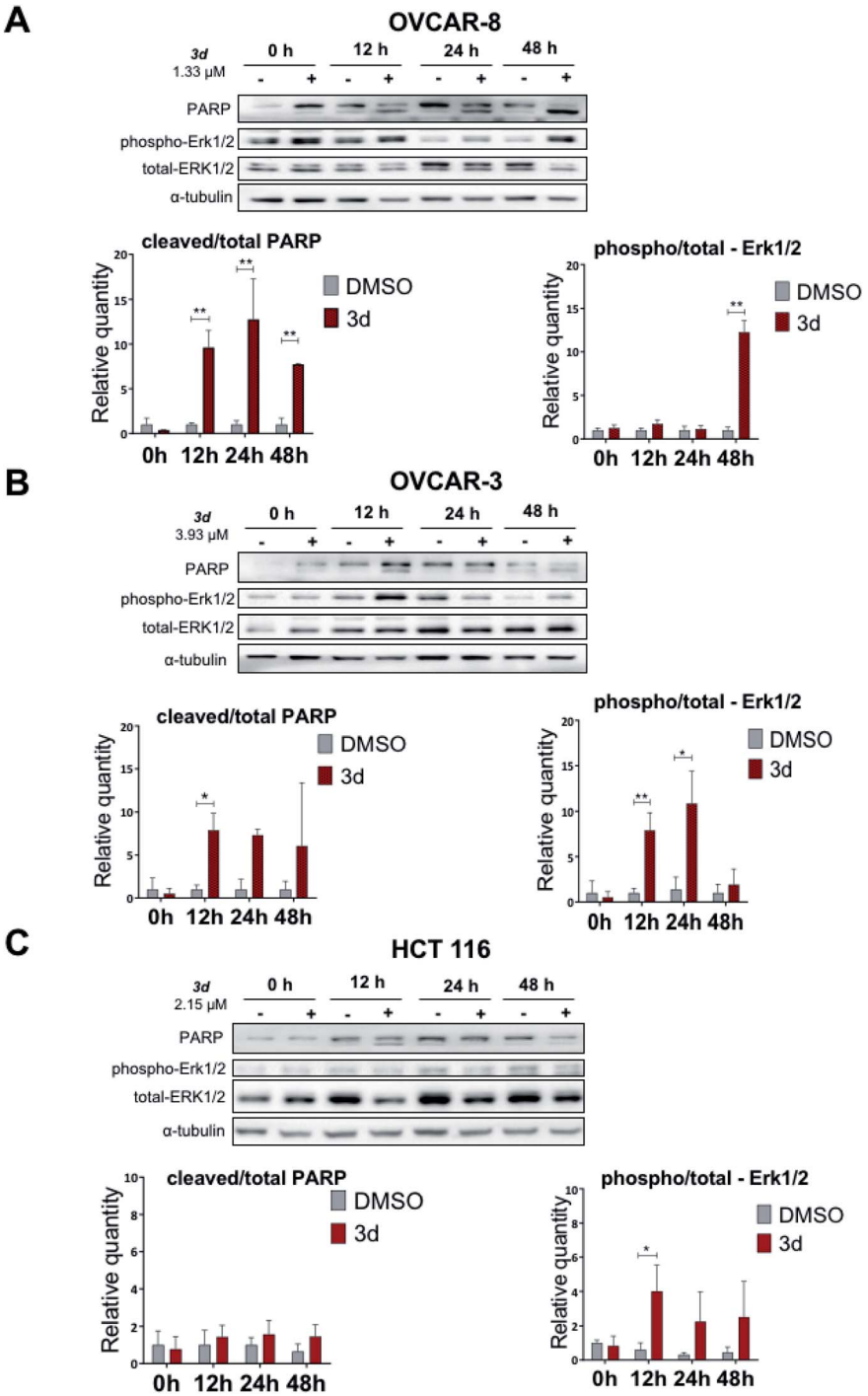

Fig. 5 Effect of the **3d** compound on apoptosis, as measured by PARP cleavage, and ERK-signaling pathway in OVCAR-8, OVCAR-3 and HCT 116 cell lines. Cells were treated with **3d** compound for 0, 12, 24 and 48 hours, and western blot analysis was done. (A) OVCAR-8 cell line; (B) OVCAR-3 cell line; (C) HCT 116 cell line.

These results confirmed that compound mixture B induces cell apoptosis in OVCAR-8 cells in a dose-dependent manner.

2.2.4. Novel tropolone compound 3d and tropolone mixture B (3i–k) induce apoptosis as measured by PARP cleavage and lead to an ERK signaling pathway activation in ovarian and colon cancer cells. Since **3d** and tropolone mixture B showed significant biologic activity as seen by suppressed proliferation and clonogenicity of cancer cells, and as were able to detect increase in apoptosis as measured by Annexin V, we next decided to elucidate whether **3d** compound and mixture B affect apoptosis and to probe their effects on a common cancer cell signaling pathway. We first investigated changes in the of PARP and ERK1/2 protein level upon **3d** treatment. PARP engages DNA repair, and genomic stability, and is one of the

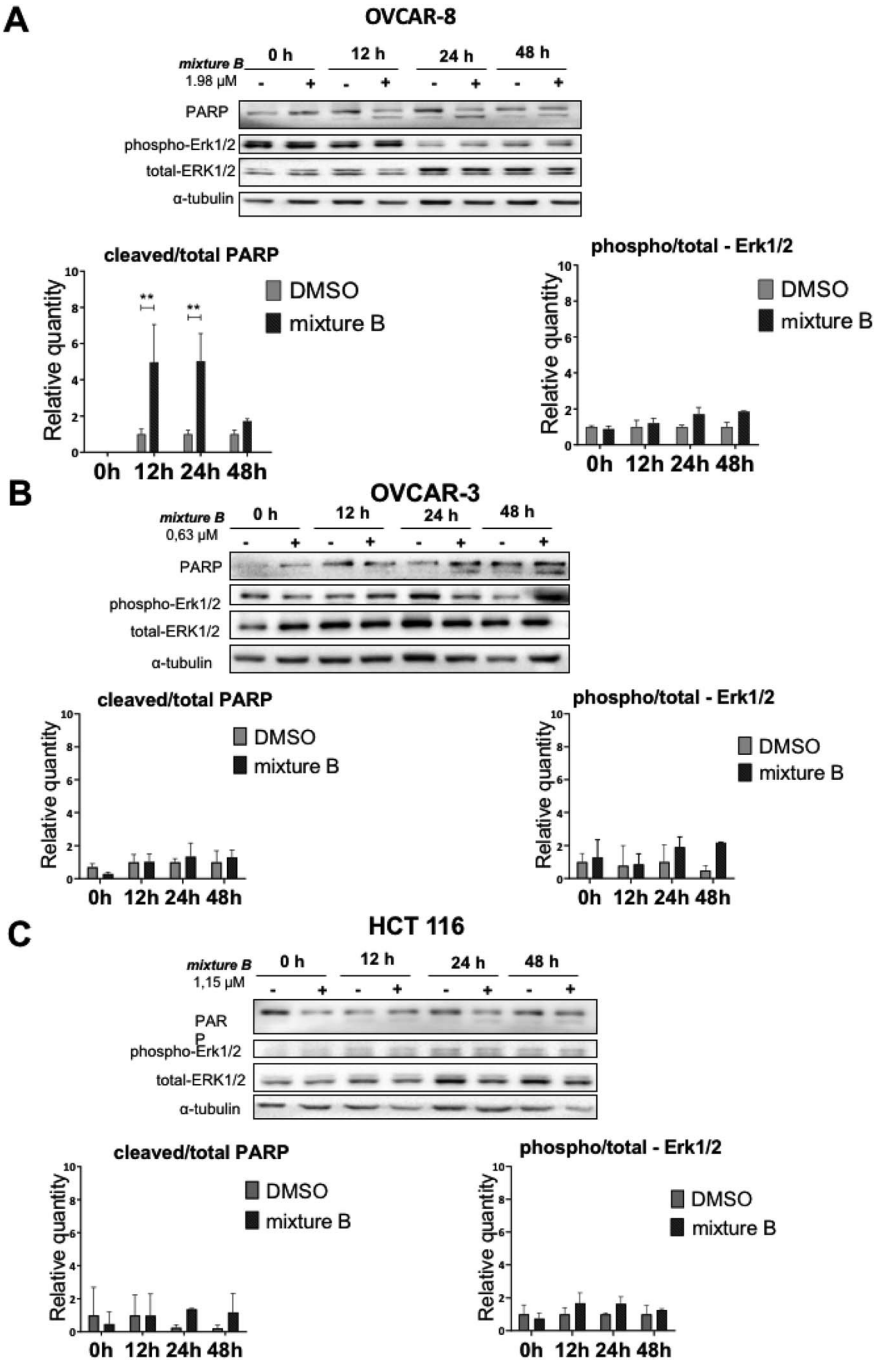

Fig. 6 Effect of the mixture B of **3i–k** compound on apoptosis, as measured by PARP cleavage and ERK-signaling pathway in OVCAR-8, OVCAR-3 and HCT 116 cell lines. Cells were treated with mixture B of **3i–k** compound for 0, 12, 24 and 48 hours. Western blot analysis: (A) OVCAR-8 cell line; (B) OVCAR-3 cell line; (C) HCT 116 cell line.

downstream proteins that is involved in programmed cell death. PARP cleavage typically indicates that this protein is inactivated, and cells are undergoing apoptosis.[31]

Here we show that the compound **3d** used at IC_{50} concentration, during incubation at different time points induces PARP cleavage in OVCAR-8, OVCAR-3 and HCT 116 cell lines, supporting our Annexin V data (Section 2.2.3) that cells are undergoing apoptosis (Fig. 5). All three cell lines were treated for 0, 12, 24 and 48 hours with **3d**, and DMSO was used as a control. In all cell lines, a statistically significant apoptosis effects appeared after 12 hours effect of **3d**. In ovarian cancer cell lines, this effect extends up to 24 hours of incubation (OVCAR-3) and up to 48 in the case of OVCAR-8 (Fig. 5).

Protein-serine/threonine kinases ERK 1/2 are involved in cell survival, proliferation, as well as adhesion and cell migration. Similar to PARP cleavage kinetics, phospho-ERK1/2 kinases

phosphorylation occurred with **3d** treatment for 12 hours. In OVCAR-3 and OVCAR-3 cell lines, high level of phospho-ERK1/2 is maintained for up to 48 hours. In the HCT 116 cell line, there was no statistically significant activation of ERK1/2-kinase, but there is a trend to increase with 48 hours of incubation (Fig. 5).

Finally, we investigated apoptosis and signaling effects of tropolone mixture B (**3i–k**) treatment, as described in Fig. 6. Cells were treated with IC_{50} concentration of mixture B for 0, 12, 24 and 48 hours. There was a significant induction of cleaved PARP between the two conditions under DMSO and mixture B in OVCAR-8 cells on 12 and 24 hours (Fig. 6A). Meanwhile, in OVCAR-3 and HCT 116 cell lines, slight non-significant increase in the cleaved/total PARP 24 and 48 hours can be clearly seen. Turning now to the experimental evidence on protein-serine/threonine kinases ERK1/2, we did not find significant ERK1/2 phosphorylation in across all three cell lines (Fig. 6A–C).

3. Conclusions

In this study, a series of novel 2-quinolyl-substituted 1,3-tropolones **3** was obtained. The structure of compounds **3** was confirmed by physicochemical methods of analysis (NMR ^{1}H, ^{13}C, IR and Mass spectrometry). The structure of 5,7-di(*tert*-butyl)-2-(4,7-dichloro-8-methyl-2-quinolyl)-4-nitro-1,3-tropolone established by X-ray analysis. The relative thermodynamic stability of (OH) and (NH) tautomeric forms of 2-quinolyl-substituted 1,3-tropolones **3** has been studied. In subsequent testing for biological activity, compound **3d** and tropolone mixture B of **3i–k** exhibited the broadest and potent activities against six various human cancer cell lines with IC_{50} values ranging from 0.63 to 3.93 μM. Furthermore, compound **3d** reduced colony formation induced apoptosis in ovarian cancer (OVCAR-3, OVCAR-8) and colon cancer (HCT 116) cell lines. However, it should be noted that when testing the effect of compounds on the ability to colony formation, tropolone mixture B of **3i–k** did not show activity, although the proliferation assay nominated it as a strong active compound. Also, cell death was induced by tropolone mixture B of **3i–k** treatment appeared only in OVCAR-8 cell line, but not in OVCAR-3 and HCT 116 as no significant changes of percent apoptotic cells and accumulation of cleaved PARP this cell line under compound treatment were detected. In summary, tropolone mixture B of **3i–k** can lead to apoptosis activation but had a narrower range of activity in this study and has less potent anti-tumor activity than **3d**. Finally, the ERK pathway was broadly induced by **3d** compound, but not by tropolone mixture B of **3i–k** treatment. Taken together, our study suggests that 2-quinolyl-1,3-tropolones are a promising new class of heterocyclic compounds that should be used for the future development of effective anticancer agents.

4. Materials and methods

4.1. General

The ^{1}H, ^{13}C NMR spectra were recorded on a Bruker Avance 600 spectrometer. The chemical shifts are given with respect to the signal of $SiMe_4$ as the internal standard. Attenuated total internal reflectance IR (ATR-IR) spectra were measured on a Varian 3100 FT-IR Excalibur Series spectrometer. HRMS were registered on a Bruker UHR-TOF MaxisTM Impact instrument. Chromatography was performed on columns packed with Al_2O_3 (Brockmann activity II–III). The melting point was measured on a Fisher–Johns apparatus. The IR and NMR spectra were recorded using equipment of the Shared Use Center "Molecular spectroscopy" of the Southern Federal University.

4.2. Synthesis

4.2.1. Synthesis of 5,7-di(*tert*-butyl)-2-(4,7-dichloro-8-methyl-2-quinolyl)-1,3-tropolone 3a (method A). A solution of 4,7-dichloro-2,8-dimethylquinoline **1a** (2.2 g, 10 mmol) and of 3,5-di(*tert*-butyl)-1,2-benzoquinone **2a** (4.4 g, 20 mmol) in glacial acetic acid (10 ml) was heated at 65–70 °C for 30 h. After cooled to the room temperature, the reaction mixture was diluted with water and extracted with dichloromethane (2 × 100 ml). The combined organic layers were washed with water (2 × 100 ml) and then dried with anhydrous Na_2SO_4 and the solvent was removed *in vacuo*. The residue was purified by alumina column chromatography with petroleum/dichloromethane (3 : 1) collecting the first bright yellow fraction ($R_f \sim 0.9$). After removal of the solvent *in vacuo*, the residue was recrystallized from propane-2-ol. Yellow crystals of **3a**. Yield 2.8 g (63%), mp 189–190 °C. IR (ν): 3117, 1644, 1623, 1586, 1494, 1462, 1455, 1409, 1378, 1364, 1330, 1271, 1240, 1188, 1149, 1087, 1017, 942, 879, 853, 822, 808, 767, 728, 691 cm^{-1}. ^{1}H NMR (600 MHz, $CDCl_3$) δ, ppm: 1.25 (9H, s, $C(CH_3)_3$), 1.38 (9H, s, $C(CH_3)_3$), 2.76 (3H, s, CH_3), 6.67 (1H, d, CH_{trop}, $J = 1.8$ Hz), 6.77 (1H, d, CH_{trop}, $J = 1.8$ Hz), 7.53 (1H, d, CH_{Ar}, $J = 8.9$ Hz), 7.94 (1H, d, CH_{Ar}, $J = 8.9$ Hz), 8.23 (1H, s, CH_{Ar}), 18.77 (1H, s, OH). ^{13}C NMR (151 MHz, $CDCl_3$) δ, ppm: 14.97, 29.95, 31.12, 37.19, 38.43, 114.37, 119.78, 122.74, 122.86, 123.18, 124.47, 127.94, 129.86, 137.41, 141.96, 144.12, 154.70, 155.59, 155.80, 173.84, 194.71. HRMS (ESI): m/z $[M–H]^-$ calcd for $C_{25}H_{26}Cl_2NO_2$: 442.1346; found: 442.1345. Calcd for $C_{25}H_{27}Cl_2NO_2$ (%): C, 67.57; H, 6.12; N, 3.15. Found (%): C, 67.38; H, 6.00; N, 3.02 (Fig. S5 and S6, ESI†).

4.2.2. Synthesis of 5,7-di(*tert*-butyl)-2-(4,7-dichloro-8-methyl-5-nitro-2-quinolyl)-1,3-tropolone 3b (method A). A solution of 4,7-dichloro-2,8-dimethyl-5-nitroquinoline **1b** (2.7 g, 10 mmol) and of 3,5-di(*tert*-butyl)-1,2-benzoquinone **2a** (4.4 g, 20 mmol) in glacial acetic acid (10 ml) was heated at 65–70 °C for 30 h. After cooling down to the room temperature, the reaction mixture was diluted with water and extracted with dichloromethane (2 × 100 ml). The combined organic layers were washed with water (2 × 100 ml) and then dried with anhydrous Na_2SO_4 and the solvent was removed *in vacuo*. The residue was purified by alumina column chromatography with petroleum/dichloromethane (3 : 1) collecting the first bright yellow fraction ($R_f \sim 0.4$). After removal of the solvent *in vacuo*, the residue was recrystallized from propane-2-ol. Yellow crystals of **3b**. Yield 2.3 g (47%), mp 264–265 °C. IR (ν): 3115, 1658, 1595, 1577, 1539, 1486, 1463, 1455, 1392, 1367, 1317, 1287, 1245, 1192, 1100, 1025, 1003, 942, 893, 872, 864, 836, 813, 763, 727, 704 cm^{-1}. ^{1}H NMR (600 MHz, $CDCl_3$) δ, ppm: 1.26 (9H, s, $C(CH_3)_3$), 1.38 (9H, s, $C(CH_3)_3$), 2.78 (3H, s, CH_3), 6.69 (1H, d,

CH_{trop}, $J = 1.8$ Hz), 6.85 (1H, d, CH_{trop}, $J = 1.8$ Hz), 7.67 (1H, s, CH_{Ar}), 8.28 (1H, s, CH_{Ar}), 17.57 (1H, s, OH). $^{13}\underline{C}$ NMR (151 MHz, $CDCl_3$) δ, ppm: 15.88, 29.95, 31.10, 37.46, 38.57, 114.41, 114.53, 123.11, 123.17, 123.81, 123.89, 135.20, 135.50, 139.96, 144.17, 145.01, 156.20, 156.43, 157.25, 171.36, 194.08. HRMS (ESI): m/z $[M–H]^-$ calcd for $C_{25}H_{25}Cl_2N_2O_4$: 487.1197; found: 487.1190. Calcd for $C_{25}H_{26}Cl_2N_2O_4$ (%): C, 61.36; H, 5.35; N, 5.72. Found (%): C, 61.12; H, 5.08; N, 5.56 (Fig. S7 and S8, ESI†).

4.2.3. Synthesis of 5,7-di(*tert*-butyl)-2-(4,7-dichloro-8-methyl-2-quinolyl)-4-nitro-1,3-tropolone 3c (method A). A solution of 4,7-dichloro-2,8-dimethylquinoline **1a** (2.2 g, 10 mmol) and of 4,6-di(*tert*-butyl)-3-nitro-1,2-benzoquinone **2b** (5.3 g, 20 mmol) in glacial acetic acid (10 ml) was heated at 65–70 °C for 15 h. After cooled to the room temperature, the reaction mixture was diluted with water and extracted with dichloromethane (2 × 100 ml). The combined organic layers were washed with water (2 × 100 ml) and then dried with anhydrous Na_2SO_4 and the solvent was removed *in vacuo*. The residue was purified by alumina column chromatography with petroleum/dichloromethane (1 : 1) collecting the second bright yellow fraction ($R_f \sim 0.6$). After removal of the solvent *in vacuo*, the residue was recrystallized from propane-2-ol. Yellow crystals of **3c**. Yield 1.45 g (30%), mp 236–237 °C. IR (ν): 3107, 1659, 1626, 1597, 1589, 1561, 1539, 1485, 1466, 1393, 1377, 1280, 1245, 1197, 1151, 1086, 1045, 1013, 966, 941, 892, 873, 851, 825, 814, 784, 767, 731, 670 cm^{-1}. $^1\underline{H}$ NMR (600 MHz, $CDCl_3$) δ, ppm: 1.28 (9H, s, $C(CH_3)_3$), 1.30 (9H, s, $C(CH_3)_3$), 2.72 (3H, s, CH_3), 6.38 (1H, s, CH_{trop}), 7.56 (1H, d, CH_{Ar}, $J = 9.0$ Hz), 7.93 (1H, d, CH_{Ar}, $J = 9.0$ Hz), 8.28 (1H, s, CH_{Ar}), 18.17 (1H, s, OH). $^{13}\underline{C}$ NMR (151 MHz, $CDCl_3$) δ, ppm: 14.67, 29.07, 30.40, 37.40, 38.01, 114.16, 118.69, 119.33, 122.11, 123.13, 126.92, 128.15, 137.73, 139.09, 143.21, 146.06, 149.96, 152.02, 154.20, 174.54, 194.09. HRMS (ESI): m/z $[M–H]^-$ calcd for $C_{25}H_{25}Cl_2N_2O_4$: 487.1197; found: 487.1193. Calcd for $C_{25}H_{26}Cl_2N_2O_4$ (%): C, 61.36; H, 5.35; N, 5.72. Found (%): C, 61.18; H, 5.10; N, 5.58 (Fig. S9 and S10, ESI†).

4.2.4. Synthesis of 5,7-di(*tert*-butyl)-2-(4,7-dichloro-8-methyl-5-nitro-2-quinolyl)-4-nitro-1,3-tropolone 3d (method A). A solution of 4,7-dichloro-2,8-dimethyl-5-nitroquinoline **1b** (2.7 g, 10 mmol) and of 4,6-di(*tert*-butyl)-3-nitro-1,2-benzoquinone **2b** (5.3 g, 20 mmol) and in glacial acetic acid (10 ml) was heated at 65–70 °C for 15 h. After cooled to the room temperature, the reaction mixture was diluted with water and extracted with dichloromethane (2 × 100 ml). The combined organic layers were washed with water (2 × 100 ml) and then dried with anhydrous Na_2SO_4 and the solvent was removed *in vacuo*. The residue was purified by alumina column chromatography with petroleum/dichloromethane (1 : 1) collecting the second bright yellow fraction ($R_f \sim 0.3$). After removal of the solvent *in vacuo*, the residue was recrystallized from propane-2-ol. Yellow crystals of **3d**. Yield 4.1 g (77%), mp 254–255 °C. IR (ν): 3111, 1664, 1602, 1547, 1490, 1464, 1366, 1329, 1281, 1244, 1199, 1096, 1053, 1020, 965, 944, 889, 869, 828, 813, 764, 735, 695 cm^{-1}. $^1\underline{H}$ NMR (600 MHz, $CDCl_3$) δ, ppm: 1.29 (9H, s, $C(CH_3)_3$), 1.31 (9H, s, $C(CH_3)_3$), 2.77 (3H, s, CH_3), 6.48 (1H, s, CH_{trop}), 7.68 (1H, s, CH_{Ar}) 8.31 (1H, s, CH_{Ar}), 18.35 (1H, s, OH). $^{13}\underline{C}$ NMR (151 MHz, $CDCl_3$) δ, ppm: 15.60, 29.06. 30.38, 37.78, 38.16, 114.49, 120.36, 122.83, 123.09, 132.25, 137.03, 140.06, 141.52, 144.94, 145.02, 148.76, 152.77, 154.59, 172.38, 193.48. HRMS (ESI): m/z $[M–H]^-$ calcd for $C_{25}H_{24}Cl_2N_3O_6$: 532.1048; found: 532.1042. Calcd for $C_{25}H_{25}Cl_2N_3O_6$ (%): C, 56.19; H, 4.72; N, 7.86. Found (%): C, 56.00; H, 4.54; N, 7.68 (Fig. S11 and S12, ESI†).

4.2.5. Synthesis of 2-(4,7-dichloro-8-methyl-5-nitro-2-quinolyl)-5,7-diisopropyl-4-nitro-1,3-tropolone 3e (method A). A solution of 4,7-dichloro-2,8-dimethyl-5-nitroquinoline **1b** (0.68 g, 2.5 mmol) and of 4,6-diisopropyl-3-nitro-1,2-benzoquinone **2c** (1.2 g, 5 mmol) and in glacial acetic acid (10 ml) was stirred for 12 h at 70 °C. After cooled to the room temperature, the reaction mixture was diluted with water and extracted with dichloromethane (2 × 100 ml). The combined organic layers were washed with water (2 × 100 ml) and then dried with anhydrous Na_2SO_4 and the solvent was removed *in vacuo*. The residue was purified by alumina column chromatography with petroleum/dichloromethane (1 : 4) collecting the second yellow fraction ($R_f \sim 0.45$). After removal of the solvent *in vacuo*, the residue was recrystallized from propane-2-ol. Yellow crystals of **3e**. Yield 0.35 g (28%), mp 255–256 °C. IR (ν): 3117, 1609, 1592, 1547, 1506, 1463, 1409, 1368, 1310, 1287, 1246, 1200, 1105, 1071, 1042, 947, 880, 841, 803, 760, 723, 692 cm^{-1}. $^1\underline{H}$ NMR (600 MHz, $CDCl_3$) δ, ppm: 1.23 (6H, d, $CH(C\underline{H}_3)_2$, $J = 6.9$ Hz), 1.24 (6H, d, $CH(C\underline{H}_3)_2$, $J = 6.9$ Hz), 2.76 (1H, sep, $C\underline{H}(CH_3)_2$, $J = 6.9$ Hz), 2.80 (3H, s, CH_3), 3.39 (1H, sep, $C\underline{H}(CH_3)_2$, $J = 6.9$ Hz), 6.49 (1H, s, CH_{trop}), 7.72 (1H, s, CH_{Ar}), 8.35 (1H, s, CH_{Ar}), 19.19 (1H, s, OH). $^{13}\underline{C}$ NMR (151 MHz, $CDCl_3$) δ, ppm: 15.76, 21.51, 22.66, 32.97, 33.49, 113.94, 114.41, 119.15, 123.66, 124.03, 133.24, 136.81, 140.45, 141.64, 143.53, 144.96, 149.53, 155.92, 158.70, 169.39, 190.02. HRMS (ESI): m/z $[M–H]^-$ calcd for $C_{23}H_{20}Cl_2N_3O_6$: 504.0735; found: 504.0725. Calcd for $C_{23}H_{21}Cl_2N_3O_6$ (%): C, 54.56; H, 4.18; N, 8.30. Found (%): C, 54.38; H, 4.02; N, 8.16 (Fig. S13 and S14, ESI†).

4.2.6. Synthesis of 2-(4,7-dichloro-8-methyl-2-quinolyl)-5,7-diisopropyl-4-nitro-1,3-tropolone 3f and 2-(4,7-dichloro-8-methyl-2-quinolyl)-5,7-diisopropyl-1,3-tropolone 3g (method A). A solution of 4,7-dichloro-2,8-dimethylquinoline **1a** (0.67 g, 3 mmol) and of 4,6-diisopropyl-3-nitro-1,2-benzoquinone **2c** (1.4 g, 6 mmol) in glacial acetic acid (10 ml) was stirred for 12 h at 70 °C. After cooled to the room temperature, the reaction mixture was diluted with water and extracted with dichloromethane (2 × 100 ml). The combined organic layers were washed with water (2 × 100 ml) and then dried with anhydrous Na_2SO_4 and the solvent was removed *in vacuo*. The residue was purified by alumina column chromatography with petroleum/dichloromethane (2 : 1) collecting the first and the second yellow fractions. The first fraction is compound **3g** ($R_f \sim 0.65$), the second fraction is compound **3f** ($R_f \sim 0.35$). After removal of the solvent *in vacuo*, the residues were recrystallized from propane-2-ol.

Yellow crystals of **3f**. Yield 0.7 g (51%), mp 189–190 °C. IR (ν): 3120, 3087, 1620, 1599, 1567, 1537, 1483, 1462, 1434, 1392, 1374, 1325, 1287, 1246, 1234, 1192, 1152, 1091, 1063, 1036, 1013, 988, 942, 889, 876, 851, 838, 825, 805, 789, 766, 722, 681 cm^{-1}. $^1\underline{H}$ NMR (600 MHz, $CDCl_3$) δ, ppm: 1.21 (6H, d, $CH(C\underline{H}_3)_2$, $J = 6.9$ Hz), 1.22 (6H, d, $CH(C\underline{H}_3)_2$, $J = 6.9$ Hz), 2.73

(1H, sep, C<u>H</u>$(CH_3)_2$, J = 6.9 Hz), 2.76 (3H, s, CH_3), 3.41 (1H, sep, C<u>H</u>$(CH_3)_2$, J = 6.9 Hz), 6.40 (1H, s, CH_{trop}), 7.60 (1H, d, CH_{Ar}, J = 8.9 Hz), 7.97 (1H, d, CH_{Ar}, J = 8.9 Hz), 8.40 (1H, s, CH_{Ar}), 19.18 (1H, s, OH). ^{13}<u>C</u> NMR (151 MHz, $CDCl_3$) δ, ppm: 14.8, 21.45, 22.64, 32.66, 33.19, 113.77, 118.11, 120.08, 122.76, 123.06, 127.71, 128.67, 138.02, 138.86, 141.50, 146.15, 151.12, 154.92, 157.75, 172.23, 190.33. HRMS (ESI): m/z $[M–H]^-$ calcd for $C_{23}H_{21}Cl_2N_2O_4$: 459.0884; found: 459.0880. Calcd for $C_{23}H_{22}Cl_2N_2O_4$ (%): C, 59.88; H, 4.81; N, 6.07. Found (%): C, 59.64; H, 4.60; N, 5.90 (Fig. S15 and S16, ESI†).

Yellow crystals of **3g**. Yield 0.12 g (10%), mp 147–148 °C. IR (ν): 3115, 3086, 1605, 1525, 1488, 1463, 1400, 1378, 1339, 1318, 1260, 1188, 1150, 1112, 1091, 1049, 1007, 990, 953, 931, 878, 865, 831, 812, 780, 769, 723, 682 cm^{-1}. ^{1}H NMR (600 MHz, $CDCl_3$) δ, ppm: 1.21 (6H, d, CH(C<u>H</u>$_3)_2$, J = 6.8 Hz), 1.24 (6H, d, CH(C<u>H</u>$_3)_2$, J = 6.8 Hz), 2.68 (1H, sep, C<u>H</u>$(CH_3)_2$, J = 6.8 Hz), 2.78 (3H, s, CH_3), 3.46 (1H, sep, C<u>H</u>$(CH_3)_2$, J = 6.8 Hz), 6.54 (1H, s, CH_{trop}), 6.65 (1H, s, CH_{trop}), 7.55 (1H, d, CH_{Ar}, J = 8.9 Hz), 7.96 (1H, d, CH_{Ar}, J = 8.9 Hz), 8.31 (1H, s, CH_{Ar}), 19.01 (1H, s, OH). ^{13}<u>C</u> NMR (151 MHz, $CDCl_3$) δ, ppm: 15.02, 22.48, 23.06, 32.64, 37.63, 115.21, 121.00, 122.72, 123.25, 125.94, 128.28, 130.28, 137.33, 141.88, 144.12, 153.08, 156.64, 157.48. HRMS (ESI): m/z $[M–H]^-$ calcd for $C_{23}H_{22}Cl_2NO_4$: 414.1033; found: 414.1034. Calcd for $C_{23}H_{23}Cl_2NO_2$ (%): C, 66.35; H, 5.57; N, 3.36. Found (%): C, 66.14; H, 5.28; N, 3.18 (Fig. S17 and S18, ESI†).

4.2.7. Synthesis of 2-(4,7-dichloro-8-methyl-2-quinolyl)-5,6,7-thrichloro-1,3-tropolone 3h (method B). To the boiling solution of 2,8-dimethyl-4,7-dichloroquinoline **1a** (1.58 g, 7 mmol) in dioxane (20 ml), portions of *o*-chloranil **2d** (1.9 g, 7.7 mmol) were added. The reaction mixture was refluxed for 20 min. After cooled to the room temperature, the yellow precipitate was filtered off, washed with dioxane. The solid was recrystallized from benzene. Yellow crystals of **3h**. Yield 2.2 g (72%), mp 275–276 °C. IR (ν): 3125, 3052, 1633, 1598, 1557, 1538, 1485, 1463, 1455, 1378, 1320, 1295, 1237, 1196, 1152, 1125, 1097, 1022, 949, 898, 881, 864, 839, 818, 767, 722, 700 cm^{-1}. ^{1}<u>H</u> NMR (600 MHz, $CDCl_3$) δ, ppm: 2.81 (3H, s, CH_3), 7.09 (1H, s, CH_{trop}), 7.64 (1H, d, CH_{Ar}, J = 9 Hz), 8.02 (1H, d, CH_{Ar}, J = 9 Hz), 8.44 (1H, s, CH_{Ar}), 19.02 (1H, s, OH). HRMS (ESI): m/z $[M–H]^-$calcd for $C_{17}H_7Cl_5NO_2$: 431.8925; found: 431.8925. Calcd for $C_{17}H_8Cl_5NO_2$ (%): C, 46.88; H, 1.85; N, 3.22. Found (%): C, 46.62; H, 1.60; N, 3.02 (Fig. S19, ESI†).

4.2.8. Synthesis of mixture of tropolones – 2-(4,7-dichloro-8-methyl-5-nitro-2-quinolyl)-5,6,7-thrichloro-1,3-tropolone 3i, 2-(4,7-dichloro-8-methyl-5-nitro-2-quinolyl)-4,5,6,7-tetrachloro-1,3-tropolone 3j and 2-(4,7-dichloro-8-methyl-5-nitro-2-quinolyl)-4,5,6-thrichloro-1,3-tropolone 3k

Method A. A solution of 4,7-dichloro-2,8-dimethyl-5-nitroquinoline **1b** (1.35 g, 5 mmol) and of *o*-chloranil **2d** (2.46 g, 10 mmol) in glacial acetic acid (15 ml) was stirred for 36 h at 50 °C. After cooled to the room temperature, the reaction mixture was diluted with water and extracted with dichloromethane (2 × 100 ml). The combined organic layers were washed with water (2 × 100 ml) and then dried with anhydrous Na_2SO_4 and the solvent was removed *in vacuo*. The residue was purified by silica gel column chromatography with dichloromethane collecting the bright yellow fraction ($R_f \sim 0.9$). After removal of the solvent *in vacuo*, the residues was recrystallized from benzene to give inseparable mixture of compounds **3i–k** (35% – **3i**, 55% – **3j** and 10% – **3k**), mp 197–200 °C (benzene) (1.4 g, yield 55%).

Method B. To the boiling solution of 4,7-dichloro-2,8-dimethyl-5-nitroquinoline **1b** (1.35 g, 5 mmol) in dioxane (20 ml) was added portions out *o*-chloranil **2d** (1.23 g, 5 mmol). The reaction mixture was refluxed for 30 min. After cooled to the room temperature and the solvent was removed *in vacuo*. The residue was purified by silica gel column chromatography with dichloromethane collecting the second bright yellow fraction ($R_f \sim 0.9$). After removal of the solvent *in vacuo*, the residues was recrystallized from benzene to give inseparable mixture of compounds **3i–k** (55% – **3i**, 30% – **3j** and 15% – **3k**), mp 192–193 °C (benzene) (1.1 g, yield 46%).

Yellow crystals of mixture of **3i–k** (method B). IR (ν): 3113, 1646, 1594, 1539, 1463, 1376, 1286, 1224, 1197, 1159, 1124, 1104, 1046, 962, 902, 885, 767, 718, 682 cm^{-1}. ^{1}<u>H</u> NMR (600 MHz, $CDCl_3$) δ, ppm: 2.83[3i] (3H, s, CH_3), 2.88[3j] (3H, s, CH_3), 2.91[3k] (3H, s, CH_3), 7.19[3i] (1H, s, CH_{trop}), 7.33[3k] (1H, s, CH_{trop}), 7.73–7.76[3i–k] (1H, m, CH_{Ar}), 8.34–8.46[3i–k] (1H, m, CH_{Ar}), 17.72[3k] (1H, s, OH), 17.92[3j] (1H, s, OH), 18.61[3i] (1H, s, OH). HRMS (ESI): $m/z$$[M–H]^-$ calcd for $C_{17}H_6Cl_5N_2O_4$ (**3i**, **3k**): 476.8774; found: 476.8777. HRMS (ESI): $m/z$$[M–H]^-$calcd for $C_{17}H_5Cl_6N_2O_4$ (**3j**): 510.8458; found: 510.8380 (Fig. S20, ESI†).

4.3. X-ray analysis

The single crystals of **3c** have been grown in dimethyl sulfoxide solution. The data collection have been performed on an Agilent SuperNova diffractometer using microfocus X-ray source with copper anode (λ = 1.54184) and Atlas S2 CCD detector. The diffraction data of **3c** were obtained at room temperature (293 K). Single crystals of $C_{25}H_{26}Cl_2N_2O_4$ are triclinic: a = 7.6690(2) Å, b = 9.8456(4) Å, c = 15.9190(6) Å, α = 88.165(3)°, β = 87.926(3)°, γ = 73.153(3)°,V = 1149.35(7) Å^3, Z = 2, T = 100 K, μ(Cu Kα) = 2.838 mm^{-1}, D_{calc} = 1.414 g cm^{-3}, space group $P\bar{1}$ (no. 2). 21 532 reflections measured (9.388° ≤ 2Θ ≤ 148.056°), 4600 unique (R_{int} = 0.0282, R_{sigma} = 0.0187) which were used in all calculations. The final R_1 was 0.0324 ($I > 2\sigma(I)$) and wR_2 was 0.0851 (all data). The collection of reflexes, determination and refinement of unit cell parameters were performed by using the specialized CrysAlisPro 1.171.38.41 software suite.[32] The structures were solved by using ShelXT program,[33] structure refinement was also performed with ShelXL program.[34] Molecular graphics were rendered and prepared for publication with the Olex2 version 1.2.10 software suite.[35] The complete X-ray diffraction datasets were deposited at the Cambridge Crystallographic Data Center (deposit CCDC 2040512) (Tables S23 and S24, ESI†).

4.4. Computational methods

All computations were carried out with Gaussian 09 (ref. 36) program package using DFT methods, employing PBE0 exchange–correlation functional[37,38] and 6-311+G(d,p) basis set. The stationary points (minima) on the potential energy surface (PES) were verified by calculating the eigenvalues of the Hessian

matrix. Solvent effects were modeled by using polarizable continuum model (PCM)[39] within the integral equation formalism (IEFPCM).[40]

4.5. Biological experiments

4.5.1. Reagents and cell lines. All tropolone compounds studied were solubilized in DMSO. OVCAR-8, OVCAR-3 and HCT 116, H441 cancer cell lines(ATCC, Manassas, VA, USA) were grown in RPMI 1640 (Gibco), A549 and Panc-1 cancercell lines were grown in DMEM (Gibco) with 10% FBS and 10 μg ml^{-1} penicillin/streptomycin solution (PanEco) with 1 μg ml^{-1} insulin (PanEco).

4.5.2. Cell viability assay. Cells were seeded into 96-well culture plates at 2000 cells per well and were grown in RPMI 1640 containing 10% FBS at 37 °C. After 24 h cells were treated with all tropolone test compounds for 72 h. After incubation, 10 μl of Alamar Blue reagent (Invitrogen, UK) was added to each well, mixed and then incubated for additional 2 hours at 37 °C in a CO_2 incubator. The fluorescence of each sample was measured using a microplate reader by fluorescence detection at excitation and emission wavelength of 540–590 nm respectively.

4.5.3. SDS–PAGE and western blot analysis. For protein analysis, cells were resuspended in a lysis RIPA buffer (#89901, Thermo, IL, USA) containing Phosphatase (#78426, Thermo, IL, USA) and Protease (#78429, Thermo) inhibitors cocktails at 4 °C, followed by the BCA protein assay (#23225, Thermo, IL, USA). Protein samples were separated electrophoretically by 15% SDS–PAGE and were then transferred to a polyvinylidene difluoride membrane (#ISEQ0001, Sigma-Aldrich, UK). The membranes were incubated with primary and secondary antibodies and then developed with enhanced chemiluminescence (#170-5061, Bio-Rad, CA, USA). The primary antibodies and their dilution factors were the 1 : 1000. For the western analysis, phospho-p44/42 MAPK (T202/Y204) (#4370S, Cell Signaling, MA, USA), p44/42 MAPK (Erk1/2) (L34F12) (#4696S, Cell Signaling, MA, USA), PARP and cleaved PARP (#9542S, Cell Signaling, MA, USA), tubulin (3873S, Cell Signaling, MA, USA) antibodies were used. For the detection of the signal from the membranes was used The ChemiDoc XRS+ System (Bio-Rad, USA) and for quantitative analysis of western blots was used Image Lab software (Bio-Rad, USA).

4.5.4. Annexin-V and PI double staining assay. Annexin-V and PI labeling for the detection of apoptotic or necrotic cell death was performed using an Alexa Fluor 488 Annexin V/Dead Cell Apoptosis Kit according to the manufacturer's instructions (Life Technologies, OR, USA). Briefly, cells were seeded in six-well plates and grown in RPMI 1640 medium containing 10% FBS at 37 °C. Cells were treated with **3d** and mixture B (**3i–k**). 1.75 μM and 1.7 μM for OVCAR-8, 3.2 μM and 0.63 μM for OVCAR-3 and 1.9 μM and 1.1 μM for HCT 116 respectively for 0 h, 24 h, 48 h. Samples were analyzed on the first (FL1) and third (FL3) detectors of the FACS Caliburcytofluometer using CellQuest software (Becton Dickinson). At least 10 000 events were calculated for each experiment.

4.5.5. Clonogenic assay. Cells (HCT 116: 500 cells per well, OVCAR-8: 2000 cells per well, OVCAR-3: 2000 cells per well) were plated in 6-well plate and incubated at 37 °C, 5% CO_2 for colony formation. On the next day cells were **3d** and mixture B (**3i–k**) with 1.75 μM and 1.7 μM for OVCAR-8, 3.2 μM and 0.63 μM for OVCAR-3 and 1.9 μM and 1.1 μM for HCT 116 respectively. After 7 days, colonies were fixed with 100% (v/v) methanol for 15 min, stained with 0.4% Crystal violet (Sigma, UK) for 30 min for colony visualization and dried. Colonies were counted using Image J software (NIH, USA).

4.6. Statistical analysis

All the data are mean values of at least 3 independent experiments and expressed as means (±SEM). For multiple-group comparison multiple *t*-tests were used by statistical software GraphPad Prism 6, *p*-value less than 0.05 was considered to be statistically significant.

Author contributions

Evgeniy A. Gusakov: methodology, investigation, data curation, visualization, writing – original draft, funding acquisition. Iuliia A. Topchu: investigation, formal analysis, data curation, visualization, writing – original draft. Aleksandra M. Mazitova: investigation, formal analysis, data curation, visualization, writing – original draft. Igor V. Dorogan: investigation, formal analysis, visualization, writing – original draft. Emil R. Bulatov: methodology, data curation, writing – original draft, funding acquisition. Ilya G. Serebriiskii: methodology, data curation, funding acquisition. Zinaida I. Abramova: methodology, investigation, data curation. Inna O. Tupaeva: investigation, data curation, visualization, writing – review & editing. Oleg P. Demidov: investigation, visualization, data curation, writing – original draft. Duong Ngoc Toan: investigation, funding acquisition. Tran Dai Lam: investigation, data curation. Duong Nghia Bang: conceptualization, investigation, data curation, visualization, writing – original draft. Yanis A. Boumber: project administration, conceptualization, investigation, writing – original draft, writing – review & editing, funding acquisition. Yurii A. Sayapin: project administration, conceptualization, investigation, writing – original draft, writing – review & editing, resources, funding acquisition. Vladimir I. Minkin: supervision, conceptualization.

Conflicts of interest

There are no conflicts to declare.

Acknowledgements

This work was financially supported by Vietnam National Foundation for Science and Technology Development "NAFOSTED" [grant 104.01-2015.68]; E. G. thanks the scholarship of the President RF [grant number SP-3728.2019.4]. Y. B. and I. T. were supported in part by the NIH R21 CA223394, NIH R01 CA218802 grants and by the NCI NIH Core Grant P30

CA060553 to the Robert H Lurie Comprehensive Cancer Center at Northwestern University. I. S. was supported by the NCI NIH Core Grant P30 CA006927 to Fox Chase Cancer Center. Yu. S. worked within the framework of the State Assignment of Southern Scientific Centre of RAS [grant number 01201354239]. E. B. was supported by RSF [grant number 19-74-10022]. Finally, this study was supported by the program for Competitive Growth of the Kazan Federal University (E. B., I. T., A. M., I. S., Z. A., and Y. B.).

References

1 R. L. Siegel, K. D. Miller and A. Jemal, *Ca-Cancer J. Clin.*, 2020, **70**(1), 7–30.
2 S. Muñoz-Galván, B. Felipe-Abrio, M. García-Carrasco, J. Domínguez-Piñol, E. Suarez-Martinez, E. M. Verdugo-Sivianes, A. Espinosa-Sánchez, L. E. Navas, D. Otero-Albiol, J. J. Marin, M. P. Jiménez-García, J. M. García-Heredia, A. G. Quiroga, P. Estevez-Garcia and A. Carnero, *J. Exp. Clin. Cancer Res.*, 2019, **38**, 234.
3 F. Bray, J. Ferlay, I. Soerjomataram, R. L. Siegel, L. A. Torre and A. Jemal, *Ca-Cancer J. Clin.*, 2018, **68**(6), 394–424.
4 L. Y. Guan and Y. Lu, *Discov. Med.*, 2018, **26**(144), 219–229.
5 K. Brasseur, N. Gévry and E. Asselin, *Oncotarget*, 2017, **8**, 4008–4042.
6 I. Mármol, J. Quero, M. J. Rodríguez-Yoldi and E. Cerrada, *Cancers*, 2019, **11**, 780.
7 A. Moreira-Paisa, R. Ferreira and R. G. da Costa, *Life Sci.*, 2018, **208**, 1–9.
8 Y. K. Lee, J. Lim, S. Y. Yoon, J. C. Joo, S. J. Park and Y. J. Park, *Int. J. Mol. Sci.*, 2019, **20**, 2443.
9 H. C. Zheng, *Oncotarget*, 2017, **8**, 59950–59964.
10 J. Zhao, *Curr. Med. Chem.*, 2007, **14**, 2597–2621.
11 Y. H. Shih, K. W. Chang, S. M. Hsia, C. C. Yu, L. J. Fuh, T. Y. Chi and T. M. Shieh, *Microbiol. Res.*, 2013, **168**, 254–262.
12 M. Elagawany, L. Hegazy, F. Cao, M. J. Donlin, N. Rath, J. Tavis and B. Elgendy, *RSC Adv.*, 2018, **8**(52), 29967–29975.
13 W. Sonyot, S. Lamlertthon, J. J. Luangsa-ard, S. Mongkolsamrit, K. Usuwanthim, K. Ingkaninan, N. Waranuch and N. Suphrom, *Antibiotics*, 2020, **9**(5), 274.
14 K. Nakano, T. Chigira, T. Miyafusa, S. Nagatoishi, J. M. M. Caaveiro and K. Tsumoto, *Sci. Rep.*, 2015, **5**, 15337.
15 H. Domon, T. Hiyoshi, T. Maekawa, D. Yonezawa, H. Tamura, S. Kawabata, K. Yanagihara, O. Kimura, E. Kunitomo and Y. Terao, *Microbiol. Immunol.*, 2019, **63**(6), 213–222.
16 S. R. Budihas, I. Gorshkova, S. Gaidamakov, A. Wamiru, M. K. Bona, M. A. Parniak, R. J. Crouch, J. B. McMahon, J. A. Beutler and S. F. J. Le Grice, *Nucleic Acids Res.*, 2005, **33**(4), 1249–1256.
17 L. Zhang, Y. Peng, I. P. Uray, J. Shen, L. Wang, X. Peng, P. H. Brown, W. Tu and G. Peng, *DNA Repair*, 2017, **60**, 89–101.
18 J. Li, E. R. Falcone, S. A. Holstein, A. C. Anderson, D. L. Wright and A. J. Wiemer, *Pharmacol. Res.*, 2016, **113**(Pt A), 438–448.
19 S. L. Haney, C. Allen, M. L. Varney, K. M. Dykstra, E. R. Falcone, S. H. Colligan, Q. Hu, A. M. Aldridge, D. L. Wright, A. J. Wiemer and S. A. Holstein, *Oncotarget*, 2017, **8**, 76085–76098.
20 C. H. Huang, S. H. Lu, C. C. Chang, P. A. Thomas, T. Jayakumar and J. R. Sheu, *Eur. J. Pharmacol.*, 2015, **746**, 148–157.
21 J. S. Seo, Y. H. Choi, J. W. Moon, H. S. Kim and S. H. Park, *BMC Cell Biol.*, 2017, **18**, 14.
22 N. Liu, W. Song, C. M. Schienebeck, M. Zhang and W. Tang, *Tetrahedron*, 2014, **70**, 9281–9305.
23 D. N. Bang, Yu. A. Sayapin, H. Lam, N. D. Duc and V. N. Komissarov, *Chem. Heterocycl. Compd.*, 2015, **51**, 291–294.
24 Yu. A. Sayapin, I. O. Tupaeva, A. A. Kolodina, E. A. Gusakov, V. N. Komissarov, I. V. Dorogan, N. I. Makarova, A. V. Metelitsa, V. V. Tkachev, S. M. Aldoshin and V. I. Minkin, *Beilstein J. Org. Chem.*, 2015, **11**, 2179–2188.
25 Yu. A. Sayapin, D. N. Bang, V. N. Komissarov, I. V. Dorogan, N. I. Makarova, I. O. Bondareva, V. V. Tkachev, G. V. Shilov, S. M. Aldoshin and V. I. Minkin, *Tetrahedron*, 2010, **66**, 8763–8771.
26 Yu. A. Sayapin, V. N. Komissarov, D. N. Bang, I. V. Dorogan, V. I. Minkin, V. V. Tkachev, G. V. Shilov, S. M. Aldoshin and V. N. Charushin, *Mendeleev Commun.*, 2008, **18**, 180–182.
27 Yu. A. Sayapin, E. A. Gusakov, I. V. Dorogan, I. O. Tupaeva, M. G. Teimurazov, N. K. Fursova, K. V. Ovchinnikov and V. I. Minkin, *Russ. J. Bioorg. Chem.*, 2016, **42**, 224–228.
28 Yu. A. Sayapin, E. A. Gusakov, A. A. Kolodina, V. N. Komissarov, I. V. Dorogan, V. V. Tkachev, G. V. Shilov, E. V. Nosova, S. M. Aldoshin, V. N. Charushin and V. I. Minkin, *Russ. Chem. Bull.*, 2014, **63**, 1364–1372.
29 Yu. A. Sayapin, D. N. Bang, E. A. Gusakov, I. V. Dorogan, V. V. Tkachev, V. S. Gorkovets, V. N. Komissarov, N. T. Duong, D. D. Nguyen, G. V. Shilov, S. M. Aldoshin and V. I. Minkin, *Russ. Chem. Bull.*, 2016, **65**, 2461–2468.
30 S. Sangher, C. Kesornpun, T. Aree, C. Mahidol, S. Ruchirawat and P. Kittakoop, *Dyes Pigm.*, 2020, **178**, 108341.
31 D. Tang, R. Kang, T. V. Berghe, P. Vandenabeele and G. Kroemer, *Cell Res.*, 2019, **29**, 347–364.
32 *CrysAlisPro, version 1.171.38.41*, Rigaku Oxford Diffraction, 2015.
33 G. M. Sheldrick, *Acta Crystallogr.*, 2008, **64**, 112–122.
34 G. M. Sheldrick, *Acta Crystallogr.*, 2015, **71**, 3–8.
35 O. V. Dolomanov, L. J. Bourhis, R. J. Gildea, J. A. K. Howard and H. Puschmann, *J. Appl. Crystallogr.*, 2009, **42**, 339–341.
36 M. J. Frisch, G. W. Trucks, H. B. Schlegel, G. E. Scuseria, M. A. Robb, J. R. Cheeseman, G. Scalmani, V. Barone, B. Mennucci, G. A. Petersson, H. Nakatsuji, M. Caricato, X. Li, H. P. Hratchian, A. F. Izmaylov, J. Bloino, G. Zheng, J. L. Sonnenberg, M. Hada, M. Ehara, K. Toyota, R. Fukuda, J. Hasegawa, M. Ishida, T. Nakajima, Y. Honda, O. Kitao, H. Nakai, T. Vreven, J. A. Montgomery Jr, J. E. Peralta, F. Ogliaro, M. Bearpark, J. J. Heyd, E. Brothers, K. N. Kudin, V. N. Staroverov, R. Kobayashi, J. Normand, K. Raghavachari, A. Rendell, J. C. Burant, S. S. Iyengar, J. Tomasi, M. Cossi, N. Rega, J. M. Millam,

M. Klene, J. E. Knox, J. B. Cross, V. Bakken, C. Adamo, J. Jaramillo, R. Gomperts, R. E. Stratmann, O. Yazyev, A. J. Austin, R. Cammi, C. Pomelli, J. W. Ochterski, R. L. Martin, K. Morokuma, V. G. Zakrzewski, G. A. Voth, P. Salvador, J. J. Dannenberg, S. Dapprich, A. D. Daniels, Ö. Farkas, J. B. Foresman, J. V. Ortiz, J. Cioslowski and D. J. Fox, *Gaussian 09, Revision A.01*, Gaussian. Inc., Wallingford CT, 2013.

37 M. Ernzerhof and G. E. J. Scuseria, *J. Chem. Phys.*, 1999, **111**, 911–915.

38 C. Adamo, G. E. Scuseria and V. J. Barone, *J. Chem. Phys.*, 1999, **111**, 2889–2899.

39 V. Barone, M. Cossi and J. Tomasi, *J. Chem. Phys.*, 1997, **107**, 3210–3221.

40 E. Cances, B. Mennucci and J. Tomasi, *J. Chem. Phys.*, 1997, **107**, 3032–3041.